

Selected Papers

Hydroxy-Functionalized Porphycenes: Structure, Spectroscopy, and Electrochemistry

Toru Okawara, Masaaki Abe,* Hisashi Shimakoshi, and Yoshio Hisaeda*

Department of Applied Chemistry, Graduate School of Engineering, Kyushu University, 744 Moto-oka, Nishi-ku, Fukuoka 819-0395

Received March 7, 2011; E-mail: mabe@mail.cstm.kyushu-u.ac.jp, yhisatcm@mail.cstm.kyushu-u.ac.jp

A series of porphycenes bearing acetoxy and hydroxy groups at the *meso*-positions have been prepared and fully characterized: H_2TPrPc-OH, [Ni(TPrPc-OH)], H_2TPrPc-OAc, and [Ni(TPrPc-OAc)], where TPrPc-OH: 9-hydroxy-2,7,12,17-tetrapropylporphycenato dianion and TPrPc-OAc: 9-acetoxy-2,7,12,17-tetrapropylporphycenato dianion. H_2TPrPc-OH is structurally determined by single-crystal X-ray diffraction, showing the *enol*-form in the solid state. The introduction of the electron-donating hydroxy group to the *meso*-position decreases the HOMO–LUMO gap by ca. 0.2 eV relative to the unsubstituted parent porphycene due to the remarkable destabilization of the HOMO level. This is experimentally confirmed by red shift of the Q band in the UV–vis spectra (in CH_2Cl_2), negative shift of the $E_{1/2}$ (in 0.1 M *n*-Bu_4NPF_6–THF), and also supported by DFT calculations. In aqueous THF, an irreversible oxidation of H_2TPrPc-OH and [Ni(TPrPc-OH)] appears to be pH-dependent, with a negative E_{pa} shift upon increasing the solution pH (in the region from 3.0 to 10.5) with slopes of −62 and −63 mV per pH unit for H_2TPrPc-OH and [Ni(TPrPc-OH)], respectively, indicating the occurrence of $\{1H^+/1e\}$ proton-coupled electron transfer.

Porphycene is a structural isomer of porphyrin prepared by Vogel and co-workers for the first time.[1] The alteration of structural symmetry from porphyrin (D_{4h}) to porphycene (D_{2h}) results in significant modulation of the electronic structure of the tetrapyrrole macrocycles, including LUMO energy stabilization,[2] remarkable increase in intensity of the Q band,[3] and tuning of the photophysical properties.[4] The coordination chemistry,[5] photophysical applications,[4,6] and biomimetic chemistry[7] of these structures have also been extensively developed. Manipulation of substituents on the porphycene backbone not only extends the synthetic diversity of the porphycene but also offers a powerful method to control their solubility, electronic structures, and reactivity. Accordingly, many peripherally functionalized porphycenes have been developed,[8] but their investigations have been mostly directed toward photosensitization for photodynamic therapy or degradation of organic pollutants.[4,6,9]

The *meso*-hydroxylated porphycene, 9-hydroxy-2,7,12,17-tetrapropylporphycene (abbreviated as H_2TPrPc-OH) (**1**) which is used for photosensitization of singlet oxygen generation,[4a,8f] is of our particular interest not only from photophysical viewpoints but also due to the potential ability to modulate the electronic structure via reversible deprotonation/protonation at the *meso*-carbon-bound oxygen under pH control. Compound **1** has been previously documented in the literature,[4a,8f] but their acid–base chemistry and the resulting pH-dependent character in aqueous media has not been reported. Such external stimuli-response characteristics may ultimately be used to create a novel porphycene-based system showing switching ability. Inspired by previous work in the literature, we have established in this work synthetic routes to **1** and its Ni^{II} complex [Ni^{II}(TPrPc-OH)] (**2**) from the precursor *meso*-acetoxyporphycenes, H_2TPrPc-OAc (**3**) and [Ni(TPrPc-OAc)] (**4**), where TPrPc-OAc: 9-acetoxy-2,7,12,17-tetrapropylporphycenato dianion. Chemical structures of porphycenes in this work are shown in Chart 1.

We present here the synthetic details and full characterization of **1**–**4**, including their electrochemical and spectroelectrochemical properties. Across the series, compound **1** was structurally determined by X-ray crystallography. We show that

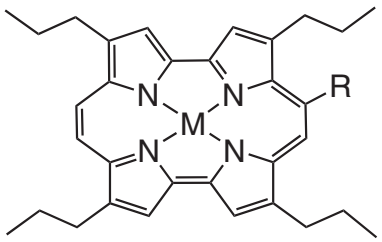

M = 2H, R = OH H_2(TPrPc-OH) **1**
M = Ni, R = OH [Ni(TPrPc-OH)] **2**
M = 2H, R = OAc H_2(TPrPc-OAc) **3**
M = Ni, R = OAc [Ni(TPrPc-OAc)] **4**

Chart 1. Schematic structures of porphycenes in this work.

Published on the web June 18, 2011; doi:10.1246/bcsj.20110072

in aqueous organic media, **1** and **2** display proton-coupled electron transfer (PCET),[10] which is the first demonstration of the pH-dependent character of porphycene-based compounds. For porphyrin systems, the *meso*-hydroxylated form is observed in the crystals of six-coordinate $[Fe^{II}(oepOH)(py)_2]\cdot 2py\cdot 0.33H_2O$ and $[Fe^{II}(CO)(N_2H_4)(oepOH)]\cdot py$,[11a] five-coordinate $[Zn^{II}(oepOH\cdot py)(py)]$,[11b] and four-coordinate $[Ni^{II}(oepOH)]$[12a] (py: pyridine and oepOH: 5-hydroxy-2,3,7,8,12,13,17,18-octaethylporphyrinato dianion), but in general, *meso*-hydroxylated porphyrins equilibrate to the *keto*-form in solution.[12]

Experimental

Materials. 2,7,12,17-Tetrapropylporphycene, H_2TPrPc,[8a] and its Ni^{II} complex, [Ni(TPrPc)][5a] were synthesized according to the literature. Spectroscopic-grade solvents, purchased from Wako Pure Chemical Industries, Ltd., were used for UV–vis spectroscopy. For electrochemical experiments, dehydrated solvents, purchased from Wako Pure Chemical Industries, Ltd., were used after N_2 purge. Tetrabutylammonium hexafluorophosphate, n-Bu_4NPF_6, was purchased from Sigma-Aldrich Co., Ltd., and used after recrystallization from ethanol. Deuterated solvents and other solvents and chemical reagents were used without further purification.

9-Acetoxy-2,7,12,17-tetrapropylporphycene (3). H_2TPrPc (151 mg, 0.314 mmol) was dissolved in a mixture of CH_2Cl_2 (16 mL) and THF (8 mL) under N_2 atmosphere. After heating to refluxing temperature, lead(IV) acetate (838 mg, 1.89 mmol) was added to the solution. The solution was refluxed for 10 min and ethylene glycol (3 mL) was added to the reaction mixture in order to halt the reaction. After cooling to room temperature, the blue solution was extracted with CH_2Cl_2 and washed twice with water. The CH_2Cl_2 solution was dried over Na_2SO_4 and evaporated under reduced pressure. The residue was subjected to silica gel chromatography by eluting with CH_2Cl_2/n-hexane (1:1, v/v). Unreacted starting material was eluted as the first band, which was confirmed by UV–vis spectrum and ESI-TOF-MS ($m/z = 479$). Compound **3** was eluted as the second band, which was collected and evaporated to dryness. Recrystallization of the residue from CH_2Cl_2/CH_3OH gave plate-like purple crystals, which were collected and dried in vacuo. Yield: 67.3 mg (0.125 mmol, 40%). ^{1}H NMR (500 MHz, $CDCl_3$): δ 9.69 (d, $J = 10$ Hz, 1H), 9.67 (d, $J = 10$ Hz, 1H), 9.43 (s, 1H), 9.25 (s, 1H), 9.24 (s, 2H), 9.20 (s, 1H), 3.96 (t, $J = 7.5$ Hz, 2H), 3.95 (t, $J = 7.5$ Hz, 2H), 3.93 (t, $J = 7.5$ Hz, 2H), 3.81 (t, $J = 7.5$ Hz, 2H), 3.64 (s, 1H), 3.17 (s, 1H), 2.83 (s, 3H), 2.36 (m, 8H), 1.33 (t, $J = 7.5$ Hz, 3H), 1.30 (t, $J = 7.5$ Hz, 3H), 1.29 (t, $J = 7.5$ Hz, 6H). IR (KBr): $\nu = 1757$ cm^{-1} (C=O). ESI-TOF-MS m/z ($M + H^+$): 537. Anal. Calcd for $C_{34}H_{40}N_4O_2$: C, 76.09; H, 7.51; N, 10.44%. Found: C, 75.69; H, 7.49; N, 10.41%.

9-Acetoxy-2,7,12,17-tetrapropylporphycenatonickel(II) (4). Compound **3** (9.2 mg, 17 μmol), nickel(II) acetate tetrahydrate (31.0 mg, 125 μmol), and sodium acetate (3.1 mg, 38 μmol) were dissolved in acetic acid (10 mL). The solution was refluxed for 1 h. After the solution was cooled to room temperature, the purple precipitates were collected by filtration and washed with cold CH_3OH. Yield: 7.4 mg (12 mmol, 73%). ^{1}H NMR (500 MHz, $CDCl_3$): δ 9.39 (d, $J = 10$ Hz, 1H), 9.33 (d, $J = 10$ Hz, 1H), 9.09 (s, 1H), 8.89 (s, 1H), 8.83 (s, 2H), 8.82 (s, 1H), 3.88 (t, $J = 7.5$ Hz, 2H), 3.87 (t, $J = 7.5$ Hz, 2H), 3.85 (t, $J = 7.5$ Hz, 2H), 3.76 (t, $J = 7.5$ Hz, 2H), 2.80 (s, 3H), 2.32 (m, 8H), 1.35 (t, $J = 7.5$ Hz, 3H), 1.33 (t, $J = 7.5$ Hz, 3H), 1.32 (t, $J = 7.5$ Hz, 6H). IR (KBr): $\nu = 1754$ cm^{-1} (C=O). ESI-TOF-MS m/z (M^+): 593. Anal. Calcd for $C_{34}H_{38}N_4NiO_2$: C, 68.82; H, 6.45; N, 9.44%. Found: C, 68.55; H, 6.43; N, 9.45%.

9-Hydroxy-2,7,12,17-tetrapropylporphycene (1). Compound **3** (8.7 mg, 16 μmol) was dissolved in dry THF (10 mL) under N_2 atmosphere. A CH_3OH solution (5 mL) of sodium methoxide (28.2 mg, 0.113 mmol) was added to the solution which was stirred for 10 min at room temperature. Water (10 mL) was poured into the reaction mixture, and then the solution was separated and the organic layer was dried over $MgSO_4$. The blue solution was evaporated and the residue was recrystallized from diethyl ether/n-heptane. Blue needle crystals were collected and dried in vacuo. Yield: 3.20 mg (6.5 μmol, 41%). ^{1}H NMR (500 MHz, THF-d_8): δ 10.38 (s, 1H), 9.51 (d, $J = 11$ Hz, 1H), 9.29 (d, $J = 11$ Hz, 1H), 9.14 (s, 1H), 9.11 (s, 4H), 4.58 (s, 1H), 4.30 (s, 1H), 3.91 (t, $J = 7.5$ Hz, 2H), 3.86 (t, $J = 7.5$ Hz, 2H), 3.84 (t, $J = 7.5$ Hz, 2H), 3.80 (t, $J = 7.5$ Hz, 2H), 2.28 (m, 8H), 1.23 (t, $J = 7.5$ Hz, 3H), 1.22 (t, $J = 7.5$ Hz, 9H). IR (KBr): $\nu = 3391$ cm^{-1} (O–H). ESI-TOF-MS m/z ($M + H^+$): 496. Anal. Calcd for $C_{32}H_{38}N_4O$: C, 77.70; H, 7.74; N, 11.33%. Found: C, 77.55; H, 7.86; N, 11.08%.

9-Hydroxy-2,7,12,17-tetrapropylporphycenatonickel(II) (2). Method 1 (Metalation of 1): Compound **1** (3.7 mg, 7.5 μmol), nickel(II) acetate tetrahydrate (13.7 mg, 55.1 μmol), and sodium acetate (1.4 mg, 17 μmol) were dissolved in acetic acid (4 mL). The solution was refluxed for 1 h. After the solution was cooled to room temperature, the dark blue precipitates were collected by filtration, washed with cold CH_3OH, and recrystallized from diethyl ether/n-heptane. Yield: 3.7 mg (6.7 μmol, 89%). ^{1}H NMR (500 MHz, THF-d_8): δ 10.11 (s, 1H), 9.32 (s, 1H), 9.12 (s, 1H), 8.98 (s, 1H), 8.79 (s, 4H), 3.95 (t, $J = 7.5$ Hz, 2H), 3.83 (s, 3H), 3.77 (s, 3H), 2.28 (m, 8H), 1.29 (m, 12H); IR (KBr): $\nu = 3543$ cm^{-1} (O–H). ESI-TOF-MS m/z (M^+): 551. Anal. Calcd for $C_{32}H_{36}N_4NiO$: C, 69.71; H, 6.58; N, 10.16%. Found: C, 69.58; H, 6.62; N, 10.07%.

Method 2 (Hydrolysis of 4): Compound **4** (20.3 mg, 34.3 μmol) was dissolved in dry THF (10 mL) under N_2 atmosphere. A CH_3OH solution (5 mL) of sodium methoxide (60.0 mg, 0.241 mmol) was added to the porphycene solution and stirred for 10 min at room temperature. Water (20 mL) was poured into the reaction mixture then the organic layer was separated and dried over Na_2SO_4. The blue solution was concentrated and recrystallized from diethyl ether/n-heptane. Yield 13.5 mg (24.4 μmol, 71%).

Instruments. UV–vis absorption spectra were recorded with a Hitachi U-3310 spectrophotometer (800–300 nm). UV–vis–NIR absorption spectra were recorded with a JASCO V-670KS spectrophotometer (1000–300 nm). ^{1}H NMR spectra were recorded at 500 MHz with a Bruker AVANCE 500 FT-NMR spectrometer using $CDCl_3$ or THF-d_8 as the solvent. TMS was used as an internal standard. IR spectra (KBr method) were obtained with a JASCO FT/IR-460 Plus spectrometer

(4000–400 cm^{-1}). Positive-mode electrospray ionization time-of-flight mass spectrometry (ESI-TOF-MS) was performed with a JEOL JMS-T100CS using CH_3OH as a solvent. Elemental analysis was carried out at the Service Centre of Elementary Analysis of Organic Compounds at Kyushu University.

X-ray Crystallography. Single crystals suitable for X-ray diffraction analysis of **1** were grown by slow evaporation of a diethyl ether/*n*-heptane solution at room temperature. A crystal with approximate dimensions $0.40 \times 0.20 \times 0.08\,mm^3$ was mounted on a glass fiber and was used for the X-ray diffraction study. Diffraction data were collected at 296 K with a Bruker SMART APEX CCD detector with graphite-monochromated Mo Kα radiation ($\lambda = 0.71073$ Å) and a 2 kW rotating anode generator to a maximum 2θ value of 18.85° in 1.49° oscillations with a 10.0 s exposure time using APEX2 [v2.1–0].[13] The crystal-to-detector distance was 50.00 mm and the detector swing angle was 28.00°. A total of 7970 reflections were collected, of which 2369 were unique ($R_{int} = 0.0887$). The structure was solved and refined using the Bruker SHELXTL Software Package[14] with a monoclinic space group $P2_1/c$ with $Z = 4$ for the formula unit $C_{32}H_{38}N_4O$. The final anisotropic full-matrix least-squares refinement on F^2 with 340 variables converged at $R_1 = 0.0836$ for the observed data and $wR_2 = 0.2389$ for all data. The goodness-of-fit was 0.954. The largest peak and hole in the final difference Fourier map were 0.500 and $-0.244\,e\,Å^{-3}$, respectively. On the basis of the final model, the calculated density was $1.193\,g\,cm^{-3}$. Hydrogen atoms on inner nitrogen were placed on all nitrogen atoms and the occupancy of the four hydrogen atoms were fixed at 0.5. CCDC-806581 contains the supplementary crystallographic data (excluding structure factors) for the structure reported in this paper. These data can be obtained free of charge via www.ccdc.cam.ac.uk/conts/retrieving.html (or from the Cambridge Crystallographic Data Centre, 12, Union Road, Cambridge, CB2 1EZ, U.K.; fax: +44 01223 336033; or deposit@ccdc.cam.ac.uk).

Electrochemistry. Cyclic voltammograms (CVs) were measured in a three-electrode cell consisting of a 3.0 mm-diameter glassy carbon or 1.6 mm-diameter platinum working electrode, a platinum coil counter electrode, and an Ag/AgCl reference electrode. Measurements were carried out with an ALS 630c instrument (ALS Co., Ltd.) placed in an N_2-filled glovebox at room temperature. CVs were recorded in 0.1 M *n*-Bu_4NPF_6–THF or CH_2Cl_2. Sample concentration was 0.2 mM. Under our experimental conditions, the redox couple of ferrocene/ferricinium (Fc/Fc^+) was observed at +0.60 V vs. Ag/AgCl for THF and +0.48 V vs. Ag/AgCl for CH_2Cl_2. To examine pH-dependent electrochemistry, a 1:1 mixture of THF and an aqueous solution containing 0.02 M of H_3PO_4, 0.02 M H_3BO_3, and 0.02 M CH_3COOH was employed as an electrolyte media. The solution pH was adjusted by adding an appropriate amount of 1 M NaOH aqueous solution. The pH was measured with a Mettler Toledo SevenMulti S40. Spectroelectrochemical studies were performed under N_2 atmosphere at room temperature with a SEC-C05 quartz glass spectroelectrochemical cell kit (ALS Co., Ltd.) consisting of platinum mesh working electrode, platinum wire counter electrode, and Ag/AgCl reference electrode.

DFT Analysis. All calculations were performed using density functional theory (DFT) at the B3LYP/6-31G* level with the Gaussian 09 package.[15] In these calculations, peripheral Pr groups were replaced by Me groups for simplicity. Optimized molecular structures and orbitals were visualized by Winmostar.[16]

Results and Discussion

Syntheses. The overall synthetic routes are shown in Scheme 1. Although **1** and **3** are known compounds, the synthetic details have not been described.[4a] All of the compounds were further characterized by elemental analysis and UV–vis and ^1H NMR spectroscopy, and **1** was structurally characterized by X-ray crystallography as described in the following sections.

The *meso*-acetoxy, free-base porphycene **3** is a precursor for the *meso*-hydroxyporphycene **1**, and was obtained by reacting H_2TPrPc with lead(IV) acetate in CH_2Cl_2/THF at refluxing temperature. Compound **3** was isolated after column chromatography and recrystallization as a crystalline solid in 40% yield. Unreacted H_2TPrPc (ca. 50% recovery) was also eluted from the column. IR spectra of **3** and **4** exhibit peaks at 1757 and 1754 cm^{-1}, respectively, due to ν(CO) of the acetoxy groups. Hydroxylation of **3** was then accomplished via hydrolysis using sodium methoxide in THF to give *meso*-hydroxyporphycene **1** in a 41% yield. Metalation of **1** and **3** with Ni^{II} ion directly gave the corresponding Ni^{II} complexes **2** (89%) and **4** (73%), respectively. Alternatively, compound **2** was also prepared via hydrolysis of **4** with sodium methoxide in 71% yield. IR spectra display ν(OH) vibrations at 3391 and 3543 cm^{-1} for **1** and **2**, respectively.

All of the compounds were further characterized by elemental analysis and UV–vis and ^1H NMR spectroscopy, and **1** was structurally determined by X-ray crystallography as described in the following sections.

X-ray Structure Analysis. The structure of **1** was determined by single-crystal X-ray diffraction analysis and the structural drawing (50% probability ellipsoids) is shown in Figure 1. Crystallographic and refinement procedures are summarized in Table 1. Selected bond distances and angles are provided in Table S1 of the SI.

Compound **1** bears a single hydroxy group directly bound to the porphycene macrocycle at the *meso*-position with C(9)–O(1) distance of 1.377(9) Å (Figure 1a, top), which is indicative of the C–O single bond of the *enol*-form in the crystalline state. This distance well compares with that found in some *meso*-hydroxyporphyrins such as $[Fe^{II}(oepOH)(py)_2]\cdot 2py\cdot 0.33H_2O$ [1.395(16) Å],[11a] $[Zn^{II}(oepOH\cdot py)(py)]$ [1.392(14) Å],[11b] $[Ni^{II}(oepOH)]$ [1.35(2) Å],[12a] and $[Co^{II}(oepOH\cdot py)(py)]$ [1.372(6) Å],[12b] but is apparently longer than that of the C=O bond (1.253(14) Å) in oxophlorin, for example, $[Co^{III}(oepO)(py)_2]$ (oepO: 2,3,7,8,12,13,17,18-octaethyl-5-oxophlorinato trianion).[12b] Similar to other free-base porphycenes, such as H_2TPrPc,[8a] the four inner nitrogen atoms in **1** form a nearly rectangular shape with N(1)···N(2) = 2.856(10), N(2)···N(3) = 2.617(9), N(3)···N(4) = 2.842(10), and N(4)···N(1) = 2.623(9) Å, which is indicative of the presence of strong hydrogen bonding between N(1) and N(4) and also between N(2) and N(3).[8a] Overall, the dimensions and

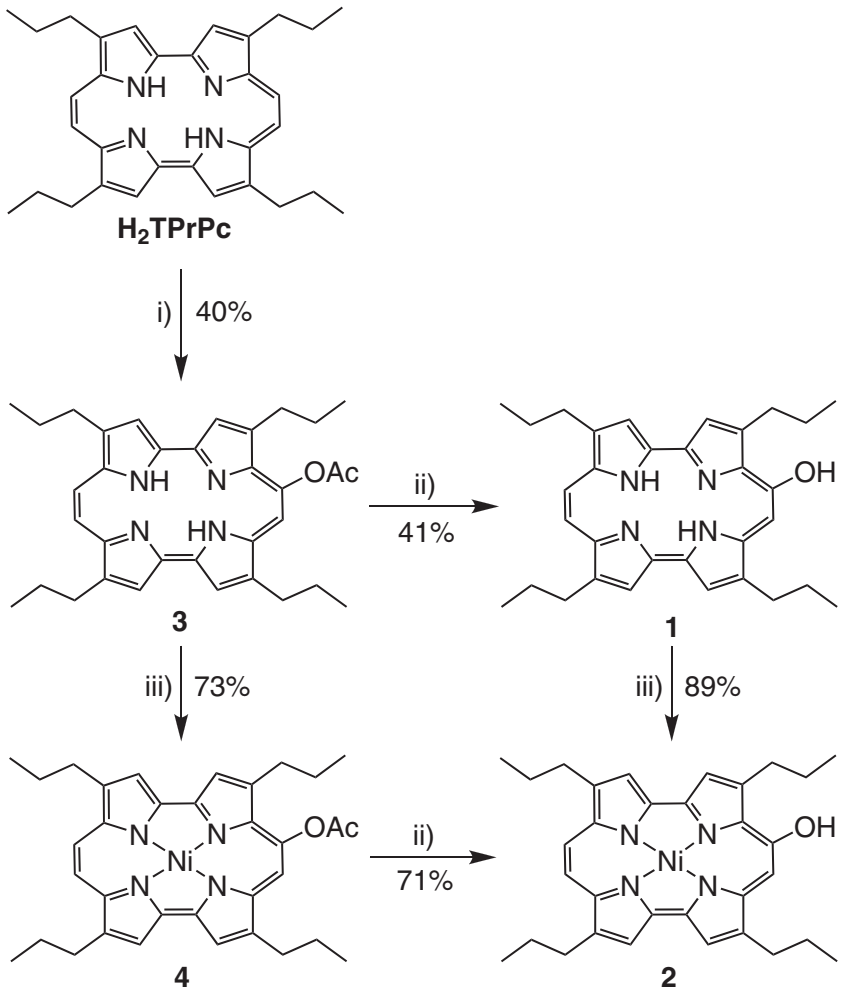

Scheme 1. Synthetic routes to *meso*-acetoxyporphycenes **3** and **4** and *meso*-hydroxyporphycenes **1** and **2**. Conditions: i) $Pb(OAc)_4$, THF/CH_2Cl_2, reflux, 10 min; ii) $NaOCH_3$, THF/CH_3OH, room temperature, 10 min; iii) $Ni(OAc)_2$, NaOAc, acetic acid, reflux, 1 h.

geometry of the porphycene ring in **1** match well those described previously for the free-base TPrPc backbone. The porphycene ring is slightly distorted from planarity (Figure 1a, bottom), where the maximum displacement of carbon from the mean plane is 0.216(7) Å. In the crystal packing diagram (Figure 1b), a face-to-face dimeric assembly is observed in which the two components are 3.407 Å apart. The pairwise motifs are arranged almost perpendicularly to each other to form a zig-zag hydrogen-bonding network via the intermolecular hydrogen-bonding C–OH···N interaction with a O···N distance of 2.950 Å and C–O···N angle of 120.0°.

^{1}H NMR Spectroscopy. Compounds **1**–**4** were characterized by ^{1}H NMR spectroscopy (details are provided in the Experimental section). The acetoxy CH_3 resonances of **3** and **4** appear as singlets at δ 2.83 (relative intensity, 3H) and 2.80 (3H), respectively, in $CDCl_3$. The presence of a single acetoxy group on the *meso*-position of the porphycene ring in **3** and **4** is indicated by unequivalent resonances due to β-pyrrole protons and *meso*-protons providing distinct chemical shifts; for **3**, two doublets ascribed to the adjacent *meso*-protons (δ 9.69 (1H) and 9.67 (1H)) and four singlets ascribed to four β-protons and an accidentally overlapping *meso*-proton (δ 9.43 (1H), 9.25 (1H), 9.24 (1H + 1H), and 9.20 (1H)). Four Pr groups in different environments are also seen as distinct resonances. The ^{1}H NMR spectra of the *meso*-hydroxyporphycenes **1** and **2** in THF-d_8 are similar to **3** and **4** except that the OH resonances appear at δ 10.38 (1H) and 10.11 (1H) as broad singlets. This assignment was confirmed by exchange with added CD_3OD.

From ^{1}H NMR chemical shift data, we suggest that **1** and **2** favor *enol*-forms over the *keto*-forms in solution as was already demonstrated in the crystal structure for **1** (see the previous section). For the porphyrin systems, it is reported that oxophlorins (e.g., the *keto*-form) show highly upfield-shifted resonances of *meso*-CH protons in the ^{1}H NMR spectra compared to the unmodified (thus aromatic) porphyrins owing to the decrease in the ring current and aromaticity of the *keto*-form of the porphyrin framework.[12a] In our porphycene case however, the *meso*-CH protons and also β-protons in **1** and **2** appear in the normal aromatic region (δ 9.51–9.11 for **1** and δ 9.32–8.79 for **2**) and the chemical shifts are compared to those for acetoxy-substituted derivatives **3** (δ 9.69–9.20) and **4** (δ 9.39–8.82) in which such tautomerism is not expected. Preference for the *enol*-form of the porphycene is probably attributed, at least in part, to its stronger hydrogen bonding within the N_4 cavity of the porphycene over the porphyrin, which may cause a decreasing capacity of porphycene to accept

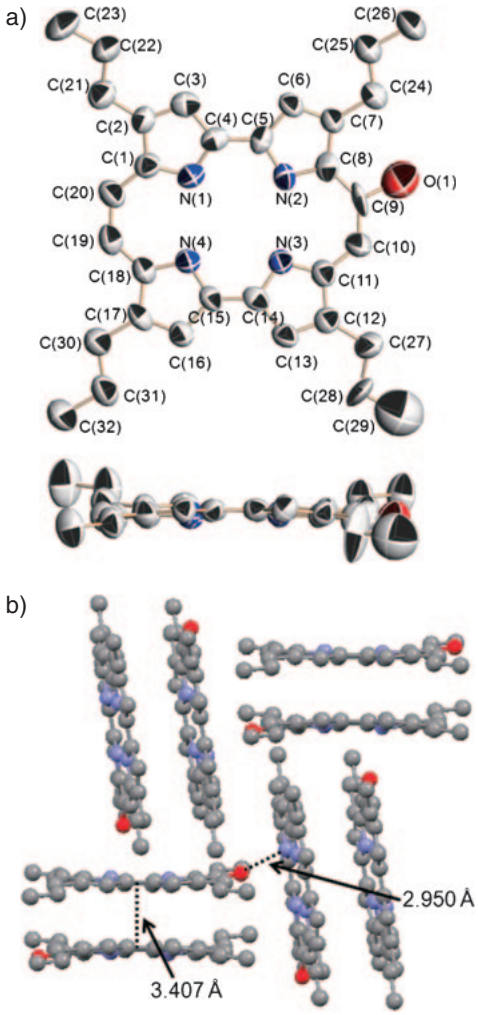

Figure 1. Crystal structure of **1**. a) ORTEP drawings of **1** with the atomic labeling in the top view (top) and the side view (bottom). Hydrogen atoms are omitted for clarity. Anisotropic displacement ellipsoids are drawn at the 50% probability level. b) A packing diagram of **1**. Broken lines indicate the intermolecular short contacts.

protons at the inner nitrogen sites to yield the putative *keto*-form of the hydroxyporphycene.

UV–vis Spectroscopy. UV–vis spectra of **1**–**4** all show strong Soret band and Q bands as shown in Figure 2. The UV–vis spectral data are collected in Table 2.

There are two principal features to be described. First, it is seen that the hydroxylation of the porphycene ring has a remarkable influence on the UV–vis absorption bands, especially on the location of the Q band. Compound **1** shows three absorption peaks at 559, 630, and 673 nm in CH_2Cl_2. The peak at the longest wavelength, 673 nm, is shifted to the longer wavelength by 40 nm compared to the non-hydroxylated porphycene, H_2TPrPc (Table 2). The extent of shift seems remarkably large in the series of substituted porphycenes.[8] Since this absorption is attributed to the transition from the HOMO to the LUMO level of the porphycene[3] the observed red shift suggests a decreasing HOMO–LUMO energy gap upon hydroxylation. An identical feature is seen for [Ni(TPrPc)][5a] ($\lambda_{max} = 600$ nm) and its hydroxylated counterpart [Ni(TPrPc-OH)] ($\lambda_{max} = 644$ nm). In contrast, the acetoxylation of the porphycene seems to have a lesser influence on the UV–vis spectra. The small influence of acetoxylation to the UV–vis spectra is also described for porphyrin systems such as octaethylporphyrin and *meso*-acetoxyoctaethylporphyrin (3 to 6 nm-red shift of the Q band).[17]

Table 1. Crystallographic and Refinement Data for **1**

Empirical formula	$C_{32}H_{38}N_4O$
Formula weight	494.66
Crystal size/mm^3	0.40 × 0.20 × 0.08
Crystal system	Monoclinic
Space group	$P2_1/c$
a/Å	15.058(4)
b/Å	11.602(3)
c/Å	17.321(5)
β/°	114.479(5)
Volume/Å^3	2754.0(13)
Z	4
Wavelength/Å	0.71073
Temperature/K	296
Density/g cm^{-3}	1.193
μ/mm^{-1}	0.073
F(000)	1064
Reflections collected	7384
Independent reflections	2164
R_{int}	0.0887
R_1[a] ($I > 2\sigma(I)$)	0.0836
wR_2[a] (all data)	0.2389
S[b]	0.954
$\Delta\rho_{max,min}$/e Å^{-3}	0.500, −0.244

a) $R_1 = \sum||F_o| - |F_c||/\sum|F_o|$, $wR_2 = [\sum w(F_o^2 - F_c^2)^2/\sum wF_o^4]^{1/2}$. b) Goodness-of-fit $S = [\sum w(F_o^2 - F_c^2)^2/(n-p)]^{1/2}$, where n is the number of reflections and p the number of parameters.

The second noticable feature in the UV–vis spectra is the overall spectral similarity of **1** and **2** to the non-hydroxylated counterparts H_2TPrPc and [Ni(TPrPc)]. This is a strong indication of the existence of **1** and **2** as their *enol*-forms in solution as was already mentioned on the basis of ^{1}H NMR spectroscopy (see above). Porphyrin systems are known to show remarkably different spectral characteristics between (aromatic) porphyrins and oxophlorins (*keto*-form), which is associated with the polyene-like electronic structure for the latter.[12f]

Titration Experiments to Determine pK_a Values. The pK_a values of the hydroxy group of **1** and **2** were determined by UV–vis spectroscopy in THF/Britton–Robinson aqueous buffer (1:1, v/v) media. The UV–vis spectra of **1** and **2** recorded at various solution pH are shown in Figure 3.

Upon increasing the solution pH from 8 to 11, **1** shows successive spectral change while maintaining isosbestic points at 345, 398, 571, 597, 657, and 683 nm, and the final spectrum (at pH 13.2) displays absorption bands at $\lambda_{max} = 361$, 411, 573, and 727 nm due to the in situ formed, deprotonated species of **1**, {H_2TPrPc-O}$^-$ (Figure 3a). Complex **2** exhibits similar pH-dependent behavior to **1** by maintaining the two-component feature and finally exhibits new peaks at $\lambda_{max} = 373$, 416, 584, and 741 nm as shown in Figure 3b. We ascribe the observed

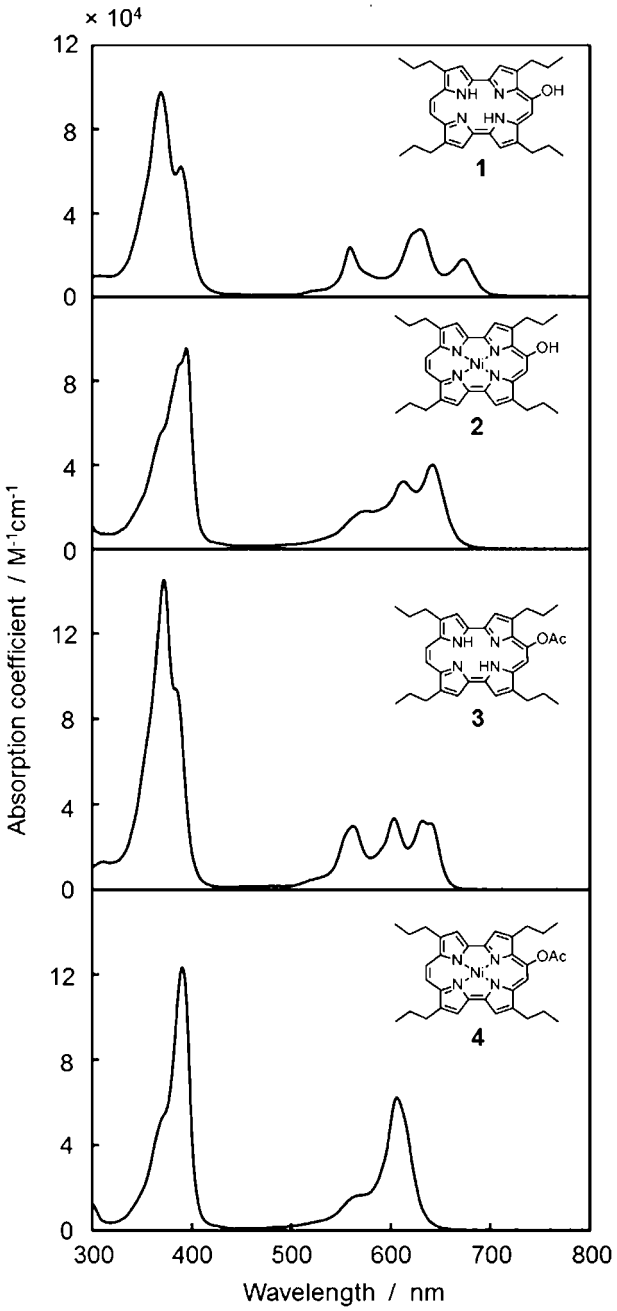

Figure 2. UV–vis spectra of **1**–**4** in CH_2Cl_2.

successive change for **1** and **2** to deprotonation of the peripheral hydroxy group as indicated by eq 1:

$$[M(TPrPc\text{-}OH)] \rightleftarrows [M(TPrPc\text{-}O)]^- + H^+ \quad M = 2H\ (\mathbf{1}),\ Ni\ (\mathbf{2}) \qquad (1)$$

From the titration curves (insets of Figure 3), the pK_a values were estimated to be 9.70 ± 0.03 and 10.76 ± 0.04 for **1** and **2**, respectively. The pK_a values obtained for **1** and **2** appear to be close to the value for phenol in water (10.09) or THF (10.68).[18] The deprotonation/protonation of the inner NH protons is unlikely in the pH region studied because of the stronger NH···N hydrogen bonding in the inner cavity of porphycene over porphyrin. The pK_a of the inner NH of the 2,3,7,8,12,13,17,18-octaethylporphyrin is reported to be 12.37 in acetonitrile.[19] The difference in pK_a of **1** and **2** may be rationalized, in part, by the higher electronegativity of hydrogen (2.20) than nickel (1.75), which leads to a lower electron density of the free-base porphycene ring than the nickel porphycene ring. This can probably lead to the higher acidity of the peripheral hydroxy group in **1** than in **2**.

An additional aspect obtained from the UV–vis data are the spectral similarity of the deprotonated species to a porphycene bearing a strongly electron-donating amino group bound to the *meso*-position. 9-Amino-2,7,12,17-tetraphenylporphycene[8b] shows two Soret bands together with a broad absorption band at 709 nm in CH_2Cl_2 which quite resembles that of the deprotonated species of **1**. This may be associated with the strong electron-donating ability for both groups (e.g., $-NH_2$ and $-O^-$).

Electrochemistry in THF. Redox properties of **1**–**4** were studied by cyclic voltammetry in THF containing 0.1 M *n*-Bu_4NPF_6 as a supporting electrolyte. Table 3 summarizes their electrochemical data.

Figures 4a and 4b show cyclic voltammograms of **1** and **2**, respectively. Free-base **1** exhibits a quasi-reversible wave at $E_{1/2} = +0.23$ V (process I) and two irreversible peaks at $E_{pc} = -1.46$ (process II) and -1.83 V (process III) (Figure 4a) which are all porphycene-based. Nickel complex **2** shows a similar behavior to **1**, somewhat increasing reversibility of waves appeared in the negative potential region (processes II and III) (Figure 4b). It is apparent from Table 3 that the electron-donating hydroxy group shifts the redox potentials negative relative to the [Ni^{II}(TPrPc)], which is most apparently revealed in the process I. This suggests that the extent of destabilization of the HOMO is more significant than that of the LUMO by the attachment of the hydroxy group. This directly causes the smaller HOMO–LUMO gap of hydroxyporphycenes than the non-hydroxylated porphycenes. The

Table 2. UV–vis Spectral Data of **1**–**4**

Compounds	λ_{max}/nm[a)] (log ε)	References
H_2TPrPc	370 (5.15), 560 (4.56), 600 (4.53), 633 (4.68)	8a
[Ni(TPrPc)]	387 (5.17), 600 (4.80)	5a
H_2TPrPc-OH (**1**)	369 (4.99), 389 (4.79), 559 (4.38), 630 (4.63), 673 (4.26)	This work
[Ni(TPrPc-OH)] (**2**)	370_{sh} (4.74), 390_{sh} (4.95), 397 (4.98), 576_{sh} (4.07), 615 (4.52), 644 (4.61)	This work
H_2TPrPc-OAc (**3**)	373 (5.16), 384_{sh} (4.97), 563 (4.97), 603 (4.52), 634 (4.51), 640 (4.49)	8f
[Ni(TPrPc-OAc)] (**4**)	371_{sh} (4.73), 390 (5.09), 571_{sh} (4.22), 606 (4.79)	This work

a) sh: shoulder.

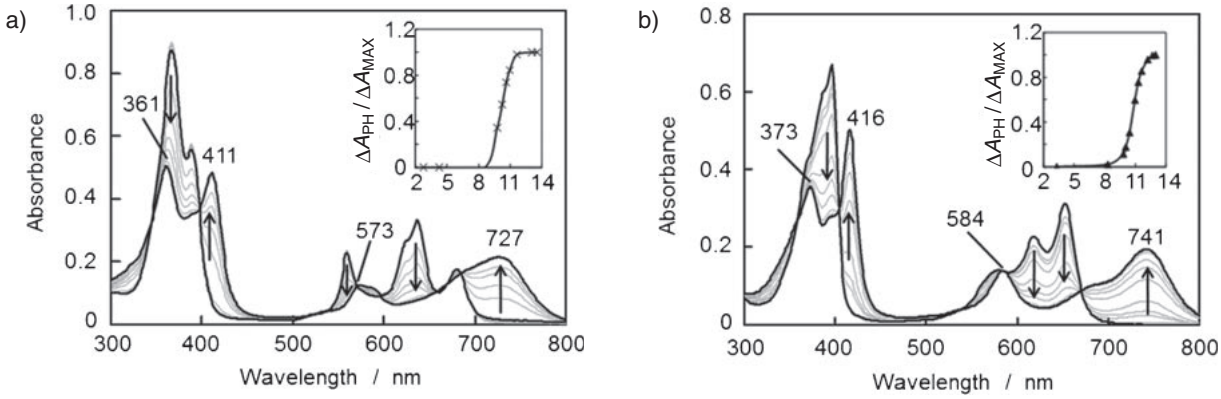

Figure 3. UV–vis spectral changes of a) **1** and b) **2** upon titration in THF/Britton–Robinson aqueous buffer solutions. Insets: titration curves recorded at 727 nm for **1** and 741 nm for **2**.

Table 3. Redox Potentials of **1**–**4** in 0.1 M n-Bu_4NPF_6–THF

Compound	Potential/V vs. Fc/Fc^+			ΔHOMO–LUMO[a] /eV
	2nd Red.	1st Red.	1st Ox.	
H_2TPrPc	−1.73	−1.40	0.53	1.93
[Ni(TPrPc)]	−1.82	−1.48	0.46	1.94
H_2TPrPc-OH (**1**)	−1.83[d]	−1.46[d]	0.23	—[e]
[Ni(TPrPc-OH)] (**2**)	−1.86	−1.53	0.22	1.75
1 + n-Bu_4NOH		−1.85[b]	−0.59	1.26[c]
2 + n-Bu_4NOH		−1.93	−0.55	1.38
H_2TPrPc-OAc (**3**)	−1.70	−1.35	0.63[b]	1.98[c]
[Ni(TPrPc-OAc)] (**4**)	−1.79	−1.42	0.47	1.89

a) $\Delta HOMO–LUMO = |E_{1/2(Red1)} - E_{1/2(Ox1)}|$. b) $E_{1/2}$ values at a scan rate of 1.00 V s^{-1}. c) Calculated from $E_{1/2}$ values at a scan rate of 1.00 V s^{-1}. d) E_{pc} values due to the irreversible processes. e) Not calculated due to poor reversibility.

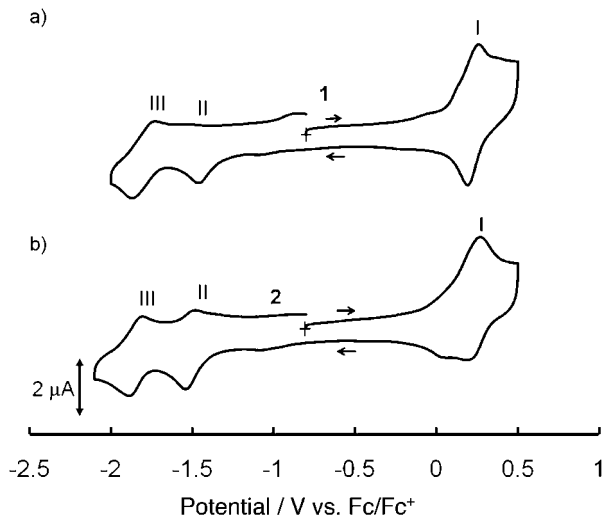

Figure 4. Cyclic voltammograms of a) **1** and b) **2** in 0.1 M n-Bu_4NPF_6–THF at room temperature. [Compound] = 0.2 mM. Scan rate = 0.1 V s^{-1}.

HOMO–LUMO gap estimated from CV is 1.75 V for **2** which is significantly smaller than that of non-hydroxylated compounds H_2TPrPc (1.93 eV) and [Ni^{II}(TPrPc)] (1.94 eV). It is seen that redox potentials of the acetoxy compounds are

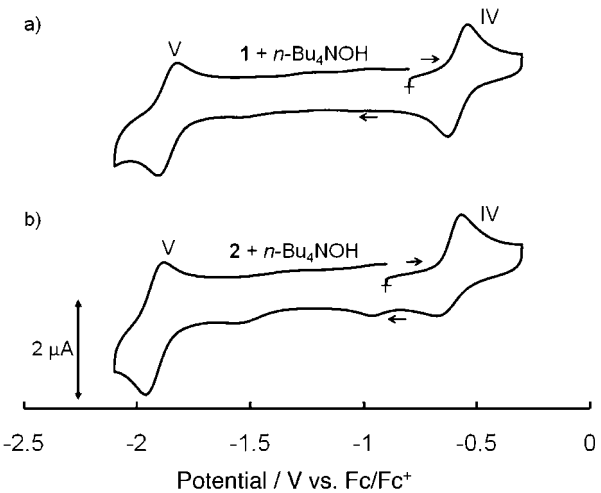

Figure 5. Cyclic voltammograms of a) **1** and b) **2** in the presence of n-Bu_4NOH (1 equivalent) in 0.1 M n-Bu_4NPF_6–THF at room temperature. [Compound] = 0.2 mM. Scan rate = 0.1 V s^{-1}.

slightly shifted to the positive region but this effect is much smaller.

We next examined the redox behavior of deprotonated species which were generated in situ by adding a base. Figure 5 shows redox waves of **1** and **2** in the presence of 1 equivalent of n-Bu_4NOH, illustrating a dramatic change in their voltammograms. As shown in Figure 5a, a negative shift of the two waves, processes IV and V, is apparent for both compounds, which are tentatively assigned to $[M(TPrPc\text{-}O)]^-$/$[M(TPrPc\text{-}O)]^{\bullet}$ and $[M(TPrPc\text{-}O)]^-$/$[M(TPrPc\text{-}O)]^{\bullet 2-}$, respectively. It is assumed that further reduction, if it may happen, is shifted beyond the potential window (e.g., potential lower than −2.5 V vs. Fc/Fc^+).

Scheme 2 depicts proposed redox processes of **1** in the absence and the presence of n-Bu_4NOH in THF media. In this scheme, compound **1** and its oxidized and reduced states are tentatively described as their "nitrogen protonated" forms; it is possible that a proton exchange event may occur between the nitrogen sites and the outer oxygen site in any of the redox states of **1**.

Acetoxy-porphycenes **3** and **4** exhibit three porphycene-based redox processes similar to **1** and **2** in the absence of base,

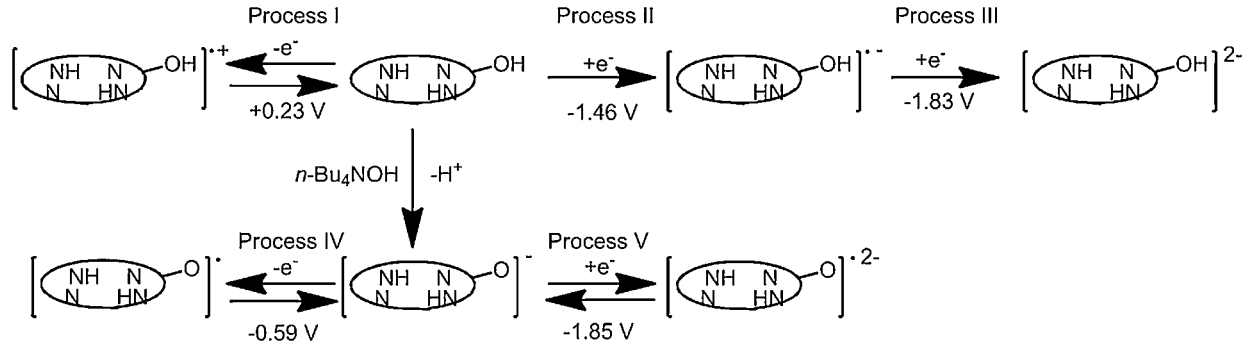

Scheme 2. Electrochemical and chemical processes of **1** in THF media.

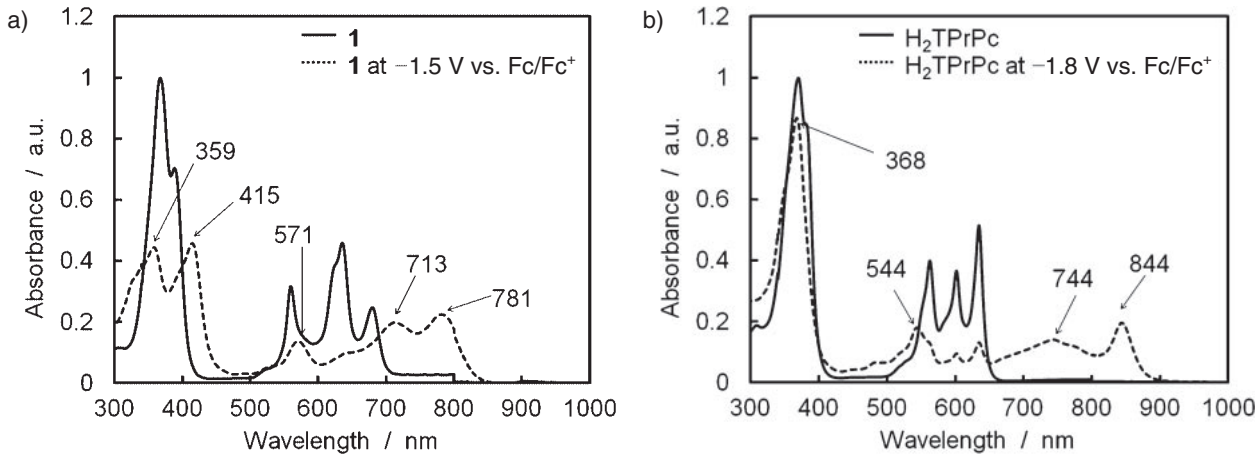

Figure 6. a) UV–vis spectra of neutral form of **1** (a solid line) and its electrochemically reduced species generated at the applied potential of −1.5 V vs. Fc/Fc^+ (a broken line). b) UV–vis spectra of neutral form of H_2TPrPc (a solid line) and its electrochemically reduced species generated at the applied potential of −1.8 V vs. Fc/Fc^+ (a broken line). All spectra were measured in 0.2 M *n*-Bu_4NPF_6–THF.

whose cyclic voltammograms recorded in a 0.1 M *n*-Bu_4NPF_6–THF and CH_2Cl_2 are provided in Figures S1 and S2, respectively, in the SI. In CH_2Cl_2, more reversible character is obtained than in THF. Positive shift of the redox potentials relative to H_2TPrPc or [Ni(TPrPc)] is attributed to the electron-withdrawing nature of the acetoxy group.

Spectroelectrochemistry. The controlled potential UV–vis–NIR spectra of **1** and H_2TPrPc were measured in 0.2 M *n*-Bu_4NPF_6–THF at room temperature under N_2 atmosphere using an optically transparent thin-layer cell with a platinum mesh working electrode, a platinum wire counter electrode, and an Ag/AgCl reference electrode. Figure 6a shows UV–vis spectra of **1** (a neutral form) and the one-electron-reduced species which was generated at applied potential −1.50 V vs. Fc/Fc^+.

Prior to electrochemical reduction, **1** shows Q-bands at $\lambda_{max} = 559$, 635, and 680 nm and the Soret band at $\lambda_{max} = 367$ and 389 nm (Figure 6a, a solid line). Upon electrochemical reduction (−1.50 V), these bands are found to be decreased in intensity and shift to longer wavelength (a broken line). This spectral feature was completely different from electrochemically generated one-electron-reduced species of H_2TPrPc at −1.80 V vs. Fc/Fc^+, as presented in Figure 6b. The Soret band of radical anion of H_2TPrPc is a little bit lower in intensity than its neutral form but does not split.[2b] Additionally, the radical anion of H_2TPrPc shows a characteristic near-IR absorption band at 844 nm. These spectral data suggest that one-electron-reduced **1**, namely $\{H_2TPrPc\text{-}OH\}^{\bullet-}$ transforms to other species over a relatively longer time scale than CVs (ca. 30 min). The reason for this transformation is under investigation.

Electrochemistry in Aqueous THF for PCET Reactions. The pH dependence of the redox behavior of **1** and **2** was examined by cyclic voltammetry using a mixed solution system, THF/Britton–Robinson aqueous buffer (1:1, v/v) which contains H_3PO_4, H_3BO_3, and CH_3COOH (all 0.02 M). The solution pH was adjusted with 1 M NaOH aqueous solution in the range between 2.5 and 13.0. Figures 7a and 7b show CVs of **1** and **2**, respectively, recorded at various pH and their potential–pH diagrams (Pourbaix diagrams), where anodic peak potential (E_{pa}) is plotted due to the irreversible character of the process.

The peak potential is found to shift linearly to negative potential with increasing solution pH until the pH reaches 10.5 and becomes independent above 10.5. As shown in Figures 7c and 7d, the slopes in the Pourbaix diagrams are found to be −62 and −63 mV per pH unit for **1** and **2**, respectively, clearly indicating that both compounds undergo one-electron/one-proton coupled transfer at $2.5 < pH < 10.5$ and one-electron transfer at > 10.5 as indicated by eqs 2 and 3, respectively. Such pH-dependent redox tuning has not been described in the literature for the porphycene system.

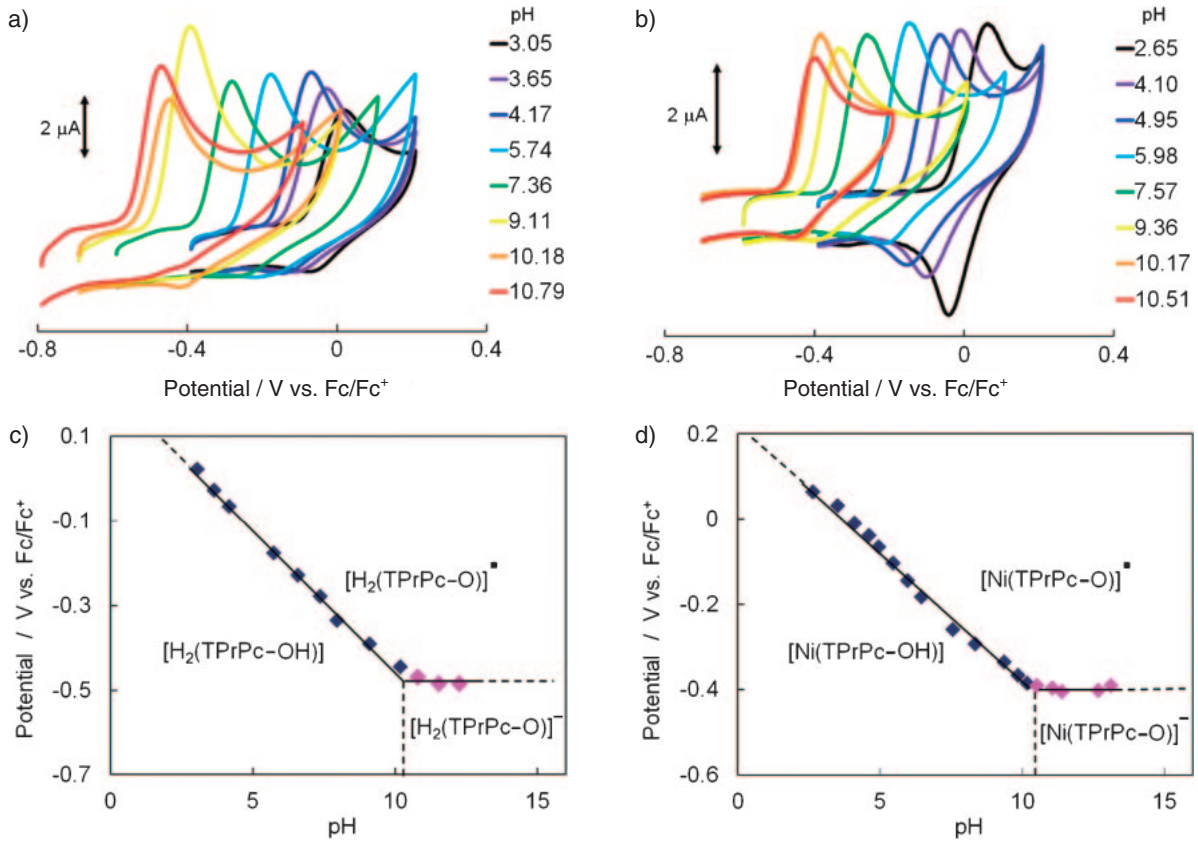

Figure 7. Cyclic voltammograms of a) **1** and b) **2** at various solution pH in THF/Britton–Robinson buffer (1:1, v/v) solution and the Pourbaix diagrams of c) **1** and d) **2**.

$$2.5 < \mathrm{pH} < 10.5\text{: } [\mathrm{M(TPrPc\text{-}OH)}] \rightarrow [\mathrm{M(TPrPc\text{-}O)}]^{\bullet} + \mathrm{H}^{+} + \mathrm{e} \quad (2)$$

$$\mathrm{pH} > 10.5\text{: } [\mathrm{M(TPrPc\text{-}O)}]^{-} \rightarrow [\mathrm{M(TPrPc\text{-}O)}]^{\bullet} + \mathrm{e} \quad (3)$$

$$(\mathrm{M} = 2\mathrm{H},\ \mathbf{1};\ \mathrm{Ni^{II}},\ \mathbf{2})$$

DFT Calculations. In order to obtain further insights into the electronic structures of **1**–**4** as well as their spectroscopic and electrochemical properties, DFT calculations have been performed using the following methyl-substituted free-base porphycenes as model compounds: 9-hydroxy-2,7,12,17-tetramethylporphycene (**1′**), 9-acetoxy-2,7,12,17-tetramethylporphycene (**3′**), and 2,7,12,17-tetramethylporphycene (H_2TMPc). The HOMO and LUMO orbitals of these model compounds are presented in Figure 8, which includes the HOMO–LUMO gaps.

For hydroxyporphycene **1′**, it is seen that the oxygen atom in the hydroxy group is well involved in the porphycene HOMO level. This seems to be in contrast to the situation of the acetoxyporphycene **3′** where a lesser extent of electron density is found on that substituent. As was already implicated experimentally (UV–vis spectroscopy and electrochemistry), the substituent effect of the hydroxy group is remarkable. The acetoxy group stabilizes both HOMO and LUMO levels weakly but the hydroxy group destabilizes them to a significant extent, especially increasing the HOMO energy level. This substituent effect makes the HOMO–LUMO gap of **1′** smaller (2.30 eV) than **3′** (2.46 eV) and H_2TMPc (2.43 eV), which corroborates the results of UV–vis spectroscopy and electrochemistry described in the previous sections.

Conclusion

In this paper, we have demonstrated the synthesis and characterization of a series of porphycenes bearing a single acetoxy group or hydroxy group at the *meso*-position, H_2TPrPc-OAc and H_2TPrPc-OH and their nickel(II) complexes, [Ni(TPrPc-OAc)] and [Ni(TPrPc-OH)]. The existence of the *meso*-hydroxyporphycene as its *enol*-form in the solid state and in solution was confirmed by single-crystal X-ray diffraction analysis and spectroscopic means including UV–vis and ^{1}H NMR, respectively. This is in remarkable contrast to known porphyrin systems where the *keto*-form (oxophlorin) is highly favored.[12] The *meso*-carbon bound hydroxy group, which displays electron-donating character, appears dramatically to affect the porphycene electronic structures, making the HOMO–LUMO gap smaller than that of the unsubstituted porphycene, which was confirmed by UV–vis and electrochemistry along with DFT calculations. The striking feature for the *meso*-hydroxyporphycenes is their proton-coupled electron-transfer behavior in aqueous/organic media, in which $1\mathrm{H}^{+}/1\mathrm{e}$ transfer is seen in the region, $3.0 < \mathrm{pH} < 10.5$. This work thus provides an unprecedented porphycene system whose electronic structures are directly tuned by the solution pH. The synthetic routes and the tunable ability of the porphycenes described here thus offer a significant possibility of these compounds as functional building blocks for useful applications. The *meso*-hydroxyporphycenes may also be a good precursor for various side-

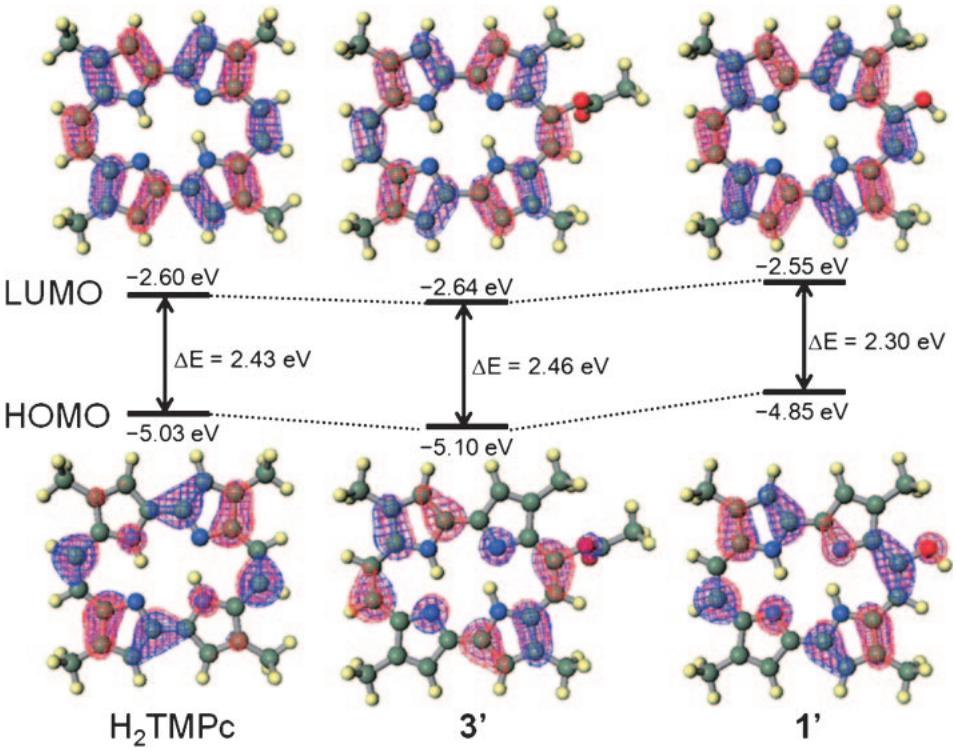

Figure 8. HOMO and LUMO orbitals of H_2TMPc, **3′**, and **1′** calculated at the B3LYP/6-31G* level with Gaussian 09 package. The orbital energies and the resulting HOMO–LUMO gaps are also included.

chain functionalizations via organic synthesis which is in progress in our laboratory.

This work was supported by Grant-in-Aid for Scientific Research on Priority Area of "Chemistry of Concerto Catalysis" (No. 18065018), "Chemistry of Coordination Space" (No. 17036002), "Coordination Programming" (No. 22108523), Grant-in-Aid for Scientific Research (A) (No. 21245016), Grant-in-Aid for Scientific Research (B) (No. 20350029), Grant-in-Aid for JSPS Fellow and the Global COE Program, "Science for Future Molecular Systems," from the Ministry of Education, Culture, Sports, Science and Technology of Japan. We also thank Tokuyama Science Foundation for financial support.

Supporting Information

Selected bond lengths and angles of **1** and cyclic voltammograms of **3** and **4**. This material is available free of charge on the Web at http://www.csj.jp/journals/bcsj/.

References

1 E. Vogel, M. Köcher, H. Schmickler, J. Lex, *Angew. Chem., Int. Ed. Engl.* **1986**, *25*, 257.

2 a) J. P. Gisselbrecht, M. Gross, M. Koecher, M. Lausmann, E. Vogel, *J. Am. Chem. Soc.* **1990**, *112*, 8618. b) C. Bernard, J. P. Gisselbrecht, M. Gross, E. Vogel, M. Lausmann, *Inorg. Chem.* **1994**, *33*, 2393. c) F. D'Souza, P. Boulas, A. M. Aukauloo, R. Guilard, M. Kisters, E. Vogel, K. M. Kadish, *J. Phys. Chem.* **1994**, *98*, 11885. d) F. D'Souza, P. L. Boulas, M. Kisters, L. Sambrotta, A. M. Aukauloo, R. Guilard, K. M. Kadish, *Inorg. Chem.* **1996**, *35*, 5743.

3 a) J. Hasegawa, K. Takata, T. Miyahara, S. Neya, M. J. Frisch, H. Nakatsuji, *J. Phys. Chem. A* **2005**, *109*, 3187. b) W. A. Oertling, W. Wu, J. J. López-Garriga, Y. Kim, C. K. Chang, *J. Am. Chem. Soc.* **1991**, *113*, 127.

4 a) S. E. Braslavsky, M. Müller, D. O. Mártire, S. Pörting, S. G. Bertolotti, S. Chakravorti, G. Koç-Weier, B. Knipp, K. Schaffner, *J. Photochem. Photobiol., B* **1997**, *40*, 191. b) H. Shimakoshi, T. Baba, Y. Iseki, I. Aritome, A. Endo, C. Adachi, Y. Hisaeda, *Chem. Commun.* **2008**, 2882. c) D. Maeda, H. Shimakoshi, M. Abe, Y. Hisaeda, *Inorg. Chem.* **2009**, *48*, 9853. d) M. Taneda, D. Maeda, H. Shimakoshi, M. Abe, Y. Hisaeda, *Bull. Chem. Soc. Jpn.* **2010**, *83*, 667.

5 a) M. W. Renner, A. Forman, W. Wu, C. K. Chang, J. Fajer, *J. Am. Chem. Soc.* **1989**, *111*, 8618. b) C. J. Fowler, J. L. Sessler, V. M. Lynch, J. Waluk, A. Gebauer, J. Lex, A. Heger, F. Zuniga-y-Rivero, E. Vogel, *Chem.—Eur. J.* **2002**, *8*, 3485. c) T. Okawara, M. Abe, H. Shimakoshi, Y. Hisaeda, *Chem. Lett.* **2008**, *37*, 906. d) L. Cuesta, E. Karnas, V. M. Lynch, P. Chen, J. Shen, K. M. Kadish, K. Ohkubo, S. Fukuzumi, J. L. Sessler, *J. Am. Chem. Soc.* **2009**, *131*, 13538. e) D. Maeda, H. Shimakoshi, M. Abe, Y. Hisaeda, *Dalton Trans.* **2009**, 140; K. Aoki, T. Goshima, Y. Kozuka, Y. Kawamori, N. Ono, Y. Hisaeda, H. D. Takagi, M. Inamo, *Dalton Trans.* **2009**, 119.

6 a) R. Bonnett, *Chem. Soc. Rev.* **1995**, *24*, 19. b) J. C. Stockert, M. Canete, A. Juarranz, A. Villanueva, R. W. Horobin, J. I. Borrell, J. Teixido, S. Nonell, *Curr. Med. Chem.* **2007**, *14*, 997. c) D. Maeda, H. Shimakoshi, M. Abe, M. Fujitsuka, T. Majima, Y. Hisaeda, *Inorg. Chem.* **2010**, *49*, 2872. d) M. Fujitsuka, H. Shimakoshi, S. Tojo, L. Cheng, D. Maeda, Y. Hisaeda, T. Majima, *J. Phys. Chem. A* **2009**, *113*, 3330. e) A. Berman, A. Michaeli, J. Feitelson, M. K. Bowman, J. R. Norris, H. Levanon,

E. Vogel, P. Koch, *J. Phys. Chem.* **1992**, *96*, 3041. f) F. D'Souza, G. R. Deviprasad, M. S. Rahman, J. Choi, *Inorg. Chem.* **1999**, *38*, 2157.

7 a) T. Matsuo, H. Dejima, S. Hirota, D. Murata, H. Sato, T. Ikegami, H. Hori, Y. Hisaeda, T. Hayashi, *J. Am. Chem. Soc.* **2004**, *126*, 16007. b) T. Hayashi, D. Murata, M. Makino, H. Sugimoto, T. Matsuo, H. Sato, Y. Shiro, Y. Hisaeda, *Inorg. Chem.* **2006**, *45*, 10530.

8 a) E. Vogel, M. Balci, K. Pramod, P. Koch, J. Lex, O. Ermer, *Angew. Chem., Int. Ed. Engl.* **1987**, *26*, 928. b) O. Arad, N. Rubio, D. Sánchez-García, J. I. Borrell, S. Nonell, *J. Porphyrins Phthalocyanines* **2009**, *13*, 376. c) E. Vogel, P. Koch, X.-L. Hou, J. Lex, M. Lausmann, M. Kisters, M. A. Aukauloo, P. Richard, R. Guilard, *Angew. Chem., Int. Ed. Engl.* **1993**, *32*, 1600. d) K. S. Anju, S. Ramakrishnan, A. P. Thomas, E. Suresh, A. Srinivasan, *Org. Lett.* **2008**, *10*, 5545. e) T. Baba, H. Shimakoshi, Y. Hisaeda, *Tetrahedron Lett.* **2004**, *45*, 5973. f) E. Vogel, M. Müller, O. Halpern, A. D. Cross, U.S. Patent, **1996**. g) D. Sánchez-García, J. L. Sessler, *Chem. Soc. Rev.* **2008**, *37*, 215.

9 a) T. Baba, H. Shimakoshi, A. Endo, C. Adachi, Y. Hisaeda, *Chem. Lett.* **2008**, *37*, 264. b) H. Shimakoshi, T. Baba, Y. Iseki, A. Endo, C. Adachi, M. Watanabe, Y. Hisaeda, *Tetrahedron Lett.* **2008**, *49*, 6198.

10 a) I. J. Rhile, T. F. Markle, H. Nagao, A. G. DiPasquale, O. P. Lam, M. A. Lockwood, K. Rotter, J. M. Mayer, *J. Am. Chem. Soc.* **2006**, *128*, 6075. b) S. Hammes-Schiffer, *Acc. Chem. Res.* **2009**, *42*, 1881. c) C. Costentin, C. Louault, M. Robert, J.-M. Savéant, *Proc. Natl. Acad. Sci. U.S.A.* **2009**, *106*, 18143. d) C. Costentin, M. Robert, J.-M. Savéant, *Acc. Chem. Res.* **2010**, *43*, 1019.

11 a) S. P. Rath, M. M. Olmstead, A. L. Balch, *Inorg. Chem.* **2004**, *43*, 6357. b) A. L. Balch, B. C. Noll, E. P. Zovinka, *J. Am. Chem. Soc.* **1992**, *114*, 3380.

12 a) A. L. Balch, B. C. Noll, S. L. Phillips, S. M. Reid, E. P. Zovinka, *Inorg. Chem.* **1993**, *32*, 4730. b) A. L. Balch, M. Mazzanti, M. M. Olmstead, *Inorg. Chem.* **1993**, *32*, 4737. c) R. Bonnett, M. J. Dimsdale, G. F. Stephenson, *J. Chem. Soc. C* **1969**, 564. d) A. L. Balch, B. C. Noll, S. M. Reid, E. P. Zovinka, *J. Am. Chem. Soc.* **1993**, *115*, 2531. e) L. J. Esdaile, M. O. Senge, D. P. Arnold, *Chem. Commun.* **2006**, 4192. f) J. H. Fuhrhop, S. Besecke, J. Subramanian, C. Mengersen, D. Riesner, *J. Am. Chem. Soc.* **1975**, *97*, 7141. g) T. D. Lash, *J. Org. Chem.* **1992**, *57*, 4312.

13 Bruker, *APEX2 v2.1-0*, Bruker AXS Inc., Madison, **2006**.

14 Bruker, *SHELXTL v6.12*, Bruker AXS Inc., Madison, **2000**.

15 M. J. Frisch, G. W. Trucks, H. B. Schlegel, G. E. Scuseria, M. A. Robb, J. R. Cheeseman, G. Scalmani, V. Barone, B. Mennucci, G. A. Petersson, H. Nakatsuji, M. Caricato, X. Li, H. P. Hratchian, A. F. Izmaylov, J. Bloino, G. Zheng, J. L. Sonnenberg, M. Hada, M. Ehara, K. Toyota, R. Fukuda, J. Hasegawa, M. Ishida, T. Nakajima, Y. Honda, O. Kitao, H. Nakai, T. Vreven, J. A. Montgomery, Jr., J. E. Peralta, F. Ogliaro, M. Bearpark, J. J. Heyd, E. Brothers, K. N. Kudin, V. N. Staroverov, R. Kobayashi, J. Normand, K. Raghavachari, A. Rendell, J. C. Burant, S. S. Iyengar, J. Tomasi, M. Cossi, N. Rega, J. M. Millam, M. Klene, J. E. Knox, J. B. Cross, V. Bakken, C. Adamo, J. Jaramillo, R. Gomperts, R. E. Stratmann, O. Yazyev, A. J. Austin, R. Cammi, C. Pomelli, J. W. Ochterski, R. L. Martin, K. Morokuma, V. G. Zakrzewski, G. A. Voth, P. Salvador, J. J. Dannenberg, S. Dapprich, A. D. Daniels, O. Farkas, J. B. Foresman, J. V. Ortiz, J. Cioslowski, D. J. Fox, *Gaussian 09 (Revision A.02)*, Gaussian, Inc., Wallingford, CT, **2009**.

16 N. Senda, *Winmostar*, v3.804p, (http://winmostar.com/); N. Senda, *Idemitsu Tech. Rep.* **2006**, *49*, 106.

17 a) Y. Zhang, P. Chen, M. Liu, *Chem.—Eur. J.* **2008**, *14*, 1793. b) M. J. Crossley, L. G. King, S. M. Pyke, *Tetrahedron* **1987**, *43*, 4569.

18 a) D. A. Pratt, R. P. Pesavento, W. A. van der Donk, *Org. Lett.* **2005**, *7*, 2735. b) K. Araki, K. Iwamoto, S. Shinkai, T. Matsuda, *Bull. Chem. Soc. Jpn.* **1990**, *63*, 3480.

19 I. Kaljurand, A. Kütt, L. Sooväli, T. Rodima, V. Mäemets, I. Leito, I. A. Koppel, *J. Org. Chem.* **2005**, *70*, 1019.